Geophysical Research Letters

RESEARCH LETTER
10.1029/2022GL101471

Variation of Fault Creep Along the Overdue Istanbul-Marmara Seismic Gap in NW Türkiye

D. Becker[1], P. Martínez-Garzón[1], C. Wollin[1], T. Kılıç[2], and M. Bohnhoff[1,3]

[1]GFZ German Research Centre for Geosciences, Potsdam, Germany, [2]Disaster and Emergency Management Presidency (AFAD), Ankara, Türkiye, [3]Department of Earth Sciences, Free University Berlin, Berlin, Germany

Key Points:

- Earthquake repeaters along the Main Marmara Fault are identified based on a newly derived homogeneous earthquake catalog spanning 15 years
- Seismic creep estimated from these repeaters is highly variable along-strike with higher creep values along the western part
- A repeating earthquake sequence showing accelerated activity after a nearby M_w 5.2 earthquake is observed

Supporting Information:

Supporting Information may be found in the online version of this article.

Correspondence to:

D. Becker,
dbecker@gfz-potsdam.de

Citation:

Becker, D., Martínez-Garzón, P., Wollin, C., Kılıç, T., & Bohnhoff, M. (2023). Variation of fault creep along the overdue Istanbul-Marmara seismic gap in NW Türkiye. *Geophysical Research Letters*, *50*, e2022GL101471. https://doi.org/10.1029/2022GL101471

Received 4 OCT 2022
Accepted 11 MAR 2023

Author Contributions:

Conceptualization: D. Becker, P. Martínez-Garzón, M. Bohnhoff
Data curation: T. Kılıç
Formal analysis: D. Becker, C. Wollin, T. Kılıç
Funding acquisition: P. Martínez-Garzón, M. Bohnhoff
Investigation: D. Becker
Methodology: D. Becker, P. Martínez-Garzón, C. Wollin, M. Bohnhoff
Project Administration: P. Martínez-Garzón, M. Bohnhoff
Software: C. Wollin
Supervision: P. Martínez-Garzón, M. Bohnhoff
Visualization: D. Becker

Abstract Strain energy from tectonic loading can be partly released through aseismic creep. Earthquake repeaters, repeatedly activated brittle fault patches surrounded by creep, indicate steady-state creep that affects the amount of seismic energy available for the next large earthquake along a plate contact. The offshore Main Marmara Fault (MMF) of the North Anatolian Fault Zone represents a seismic gap capable of generating a $M > 7$ earthquake in direct vicinity to the mega-city Istanbul. Based on a newly compiled seismicity catalog, we identify repeating earthquakes to resolve the spatial creep variability along the MMF during a 15-year period. We observe a maximum of seismic repeaters indicating creep along the central and western MMF segments tapering off toward the locked onshore Ganos fault in the west, and the locked offshore Princes Islands segment immediately south of Istanbul in the east. This indicates a high degree of spatial creep variability along the Istanbul-Marmara seismic gap.

Plain Language Summary The relative motion of tectonic plates deforms these plates along their contact zone until the plate contact ruptures in an earthquake. However, some of this deformation can be released without earthquakes by so-called aseismic creep in which the plates creep past each other. Within this creep zone, sometimes some brittle patches exist that interlock during the plate creep and rupture repeatedly in smaller earthquakes that are very similar. They are called earthquake repeaters. In the Sea of Marmara south of Istanbul lies the contact between the Eurasian and the Anatolian plates, the so-called Main Marmara Fault (MMF). This plate contact did not rupture for a long time and thus a large magnitude event is expected here. We observe a large number of earthquake repeaters in the western offshore part of the MMF while no earthquake repeaters are found toward the east south of Istanbul or onshore toward the west. These areas seem to be locked and might accumulate deformation for a future large earthquake. The zones in between show an intermediate behavior with fewer earthquake repeaters indicating less creep. These results are important for the seismic risk and hazard assessment for the mega-city of Istanbul.

1. Introduction

The North Anatolian continental transform Fault Zone (NAFZ) bounds the Anatolian and Eurasian plates over a distance of about 1,500 km between the Karliova triple junction in the east and the Northern Aegean in the west (e.g., A. A. Barka, 1992; Bohnhoff et al., 2016; Sengör et al., 2005; Figure 1). The NAFZ reflects the westward movement of Anatolia and evolved in the framework of the northward moving Arabian plate in the east and the southward pull due to slab-rollback of the Hellenic Subduction Zone (HSZ) in the west (Bohnhoff et al., 2005; Bulut et al., 2012; Flerit et al., 2004; Le Pichon et al., 2016). The Main Marmara Fault (MMF) is the offshore part of the NAFZ in the Sea of Marmara and constitutes a seismic gap in direct vicinity to the 15-million population center of Istanbul that ruptured last in 1766 in a $M \sim 7.4$ event.

From studies of historical catalogs the estimated return period of a $M > 7$ event in this region is on the order of 250 years (Bohnhoff et al., 2016; Murru et al., 2016; Parsons, 2004). All other segments of the NAFZ ruptured during the 20th century. The sequence initiated with the 1912 M_w 7.4 Ganos event west of the Sea of Marmara and then continued with a westward migration of $M > 7$ events starting in 1939 in the East with the M_w 8.0 Erzincan earthquake and terminated in 1999 with the M_w 7.4 Izmit and M_w 7.1 Düzce events immediately east of the MMF (e.g., A. Barka et al., 2002; Reilinger et al., 2000; Stein et al., 1997; Figure 1). The question whether the overdue MMF is completely locked or partly creeping has significant consequences for the maximum expected magnitude and rupture dynamics (directivity toward or away from Istanbul) of a pending large earthquake. This largely defines the seismic hazard and subsequent risk threatening Istanbul.

Writing – original draft: D. Becker
Writing – review & editing: D. Becker, P. Martínez-Garzón, C. Wollin, T. Kılıç, M. Bohnhoff

Offshore geodetic studies identified significant creep at the Western High segment of the MMF (Yamamoto et al., 2019) while a comparable study by Lange et al. (2019) west of Istanbul identified a locked plate contact. Onshore geodetic studies suggested a locked Ganos fault toward the west of the MMF and confirmed a locked status of the offshore Princes Islands segment immediately south of Istanbul (Ergintav et al., 2014) as proposed earlier based on absence of microseismicity (Bohnhoff et al., 2013). The presence of creeping sections is often explained by weak material on the faults' principal slip surface, for example, fault gauge and/or the existence of serpentinite (e.g., Kaduri et al., 2016; Moore & Lockner, 2013). Along-fault variation of creeping or locked fault segments may also originate from lower crustal/upper mantle structure and mechanics (see e.g., Avouac, 2015). For the MMF it has been suggested that a decoupling of mechanically weaker crustal domains from the mantle is responsible for the creeping sections (Gholamrezaie et al., 2021).

The occurrence of repeating earthquakes (in the following termed "repeaters") represents re-activation of the same fault patch in quasi-periodic co-located events with the same source mechanism and comparable magnitude. Repeaters are generally interpreted as an indication for fault creep (Liu et al., 2022; Poupinet et al., 1984; Uchida & Bürgmann, 2019). They present the brittle failure of asperities surrounded by creeping areas where the asperities occupy only a small fraction of the overall fault plane. If fault creep accommodates a substantial fraction of the large-scale plate motion during the interseismic cycle, then the amount of elastic energy available for a future large earthquake decreases and a rupture initiation within this area is less likely (Harris, 2017). Along the western part of the MMF below the Central Basin and at the Western High (Figure 1), earlier studies identified several repeating earthquake sequences of different characteristics (Bohnhoff, Wollin, et al., 2017; Schmittbuhl et al., 2016; Uchida et al., 2019; Figure 1b). These studies found either repeater sequences with up to three events along the MMF using strict criteria investigating the time intervals from 2006 to 2010 (Bohnhoff, Wollin, et al., 2017) and 2005–2013 (Uchida et al., 2019), respectively, or similar events concentrated mainly on the Central Basin region investigating the time interval 2008–2015 (Schmittbuhl et al., 2016). In this study, we systematically search for repeating earthquakes utilizing a novel high-quality seismicity catalog consistently covering the entire Marmara region over a 15-year time period.

2. Data and Methods

2.1. Earthquake Data

We generated a newly assembled consistent regional earthquake catalog for the Marmara region spanning 15 years (1 January 2006–31 December 2020, black dots in Figure 1d) by extending the catalog of Wollin et al. (2018) until the end of 2020. A total of 59,714 *P*-wave picks and 35,966 *S*-wave picks were detected for the 4,327 new events with local magnitudes (M_L) between M_L 0.5 and M_L 5.7 (Text S1 in Supporting Information S1). Together with the already available 121,740 *P*-wave and 68,606 *S*-wave picks and subsequently derived 9,485 events for the time period 2006–2015 (Wollin et al., 2018) this led to a newly compiled seismicity catalog for the time period 2006–2020, composed of 13,812 unique events to be used for consistent repeater search (Becker et al., 2023). All these events were newly located using the NLLoc software (Lomax et al., 2000, 2009) using Octtree search mode (see Figures S1–S3 in Supporting Information S1 for velocity model and location uncertainties).

2.2. Repeater Identification

To identify potential repeating earthquakes along the MMF, we divided the fault trace into seven overlapping sections (Figure 1d). In addition, we investigated two further fault sections off the MMF with pronounced seismicity at the Armutlu Peninsula (AP) and in the Gulf of Gemlik (GG) for comparison (Figure 1d). We defined events as belonging to a repeater sequence if there is at least one other event in the sequence with which they share a minimum of three normalized cross correlation coefficients >0.9 calculated over the complete *P*- and *S*-wave train filtered between 2 and 20 Hz and if the time separation between the first and last sequence member is longer than 1 year. No a priori constraint for the magnitude difference is applied. For details see Text S2 in Supporting Information S1.

To determine whether the identified repeater events ruptured the same fault patch, we perform a relative relocation of events belonging to the same repeater sequence using hypoDD (Waldhauser & Ellsworth, 2000) employing cross correlation and catalog time differences (Text S2 in Supporting Information S1). The median formal errors of the successfully located events are 11, 13 and 47 m in longitude, latitude and depth, respectively. As we expect the faulting style of most of the events to be in conjunction with the MMF (right-lateral near vertical EW-striking fault plane), we assumed a vertical rupture orientation in the *x*–*z*-plane.We calculated rupture areas of

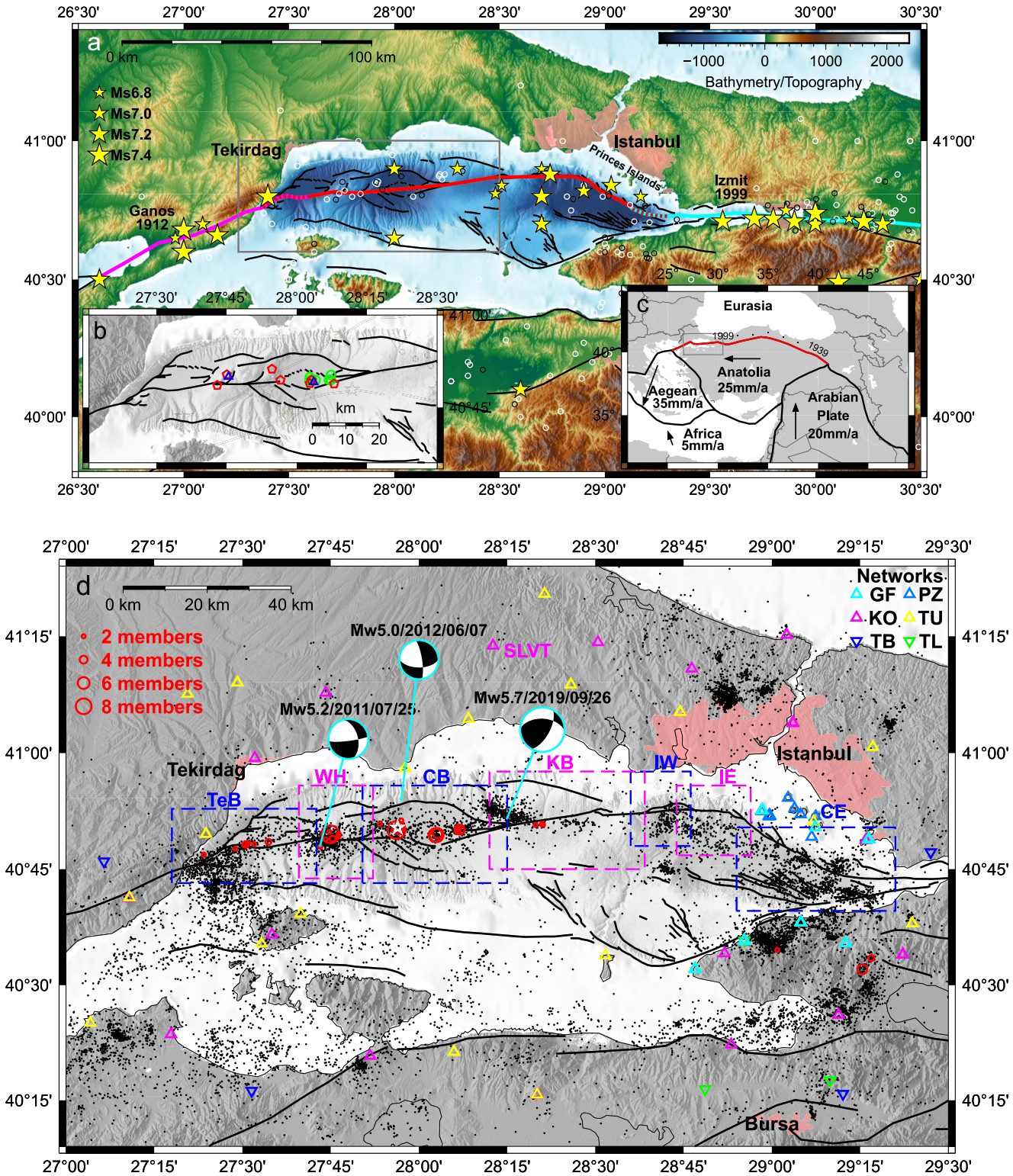

Figure 1.

the individual repeater events based on the Brune model (Brune, 1970), the Madariaga model (Madariaga, 1976) and an empirical relationship between moment magnitude and rupture area for crustal earthquakes (Bohnhoff et al., 2010, their Table 1, see also Text S2 in Supporting Information S1) and visualized the overlap by centering them around the successfully relocated hypocenters. All models resulted in rupture radii significantly larger than

the hypocentral separation of the relocated events, indicating a significant overlap of the respective rupture areas of individual repeaters of a sequence and thus a repeated activation of the same respective fault patch (for an example of a repeater sequence see Figure 2). This is an important characteristic supporting that these sequences are indeed representing repeating earthquakes (e.g., Ellsworth, 1995; Waldhauser & Schaff, 2021).

3. Results

3.1. Identified Repeater Sequences

We identify 30 earthquake repeater sequences with a total of 101 individual events in the magnitude range [1.7–3.5] and a median value of M2.6 along the MMF (Figure 1d, Table S1 in Supporting Information S1). In addition, we identify an even larger number of "burst-type" similar event sequences with an activity period <1 year along the entire MMF that we do not include in the repeater analysis (Text S2 and Figure S4 in Supporting Information S1). The number of repeaters comprising the sequences ranges from 2 to 9. The repeater sequence centroids closely follow the mapped seafloor trace of the MMF suggesting that they are reflecting fault creep on the main NAFZ branch. Out of the 30 repeater sequences, 17 contain only two members. However, a total of 13 larger sequences are observed, of which 4, 2, and 2 sequences contain 5, 7, and 9 repeater events, respectively. Due to lack of common recording stations for some sequence members and limited signal-to-noise ratios for several events, we were only able to perform a successful hypoDD relative relocation for 18 out of the 30 repeater sequences. We were able to relocate all sequences with five or more members although some events were lost during the relocation procedure due to insufficient linkage. The obtained relative relocations of repeater sequences indicate a high spatial proximity of the event members comprising the repeater sequences with a median hypocentral offset of <50 m from the respective repeater sequence centroid (e.g., see Figures 2b–2d). For the other 12 sequences we were able to verify the rupture area overlap by applying the DTDD relative event relocation technique (Gao et al., 2021; see Text S2 and Figures S5–S8 in Supporting Information S1).

3.2. Spatial Distribution of Repeater Sequences

Strikingly, nearly all the repeater sequences occur along the western portion of the MMF, with 13 sequences located in the Central Basin, and seven sequences each in the Western High and the Tekirdağ Basin (Figure 3). Toward the east, only three repeater sequences were identified, all of which are located in the Kumburgaz Basin (and none along the Princes Islands segment which is considered to be locked). Sequences with four or more members are exclusively found in the Central Basin and Western High (Figure 3). At the AP and GG sections three sequences fulfilling the repeater criteria were found. Two of them are spatially linked with a known mining area; they could likely belong to quarry blast events.

For the areas in the western part of the MMF where earthquake repeaters were reported earlier (Bohnhoff, Wollin, et al., 2017; Schmittbuhl et al., 2016; Uchida et al., 2019), the completeness magnitude is time dependent (Figure 3), with progressively smaller completeness magnitude, Mc, with time due to network geometry improvements. This indicates that some repeater sequences or sequence members might have remained undetected during earlier times. Although we did not require a homogeneity of the repeater magnitudes a priori, most of the sequences show very comparable magnitudes amongst their members.

Figure 1. Seismicity and mapped surface fault traces in the Marmara region. (a) Rupture traces of the M_w 7.4 1912 Ganos (magenta) and the M_w 7.4 1999 Izmit earthquakes (cyan), their disputed termination (dotted lines), and the Main Marmara Fault (MMF) representing an overdue seismic gap (red line). Seismicity with $M > 4.5$ since 1922 included in KOERI catalog (Kandilli Observatory and Earthquake Research Institute, 2022) and all seismicity reported by the ISC-GEM catalog between 1964 and 2018 (Di Giacomo et al., 2018; International Seismological Centre, 2022; Storchak et al., 2013, 2015) are indicated by white and black circles, respectively. Yellow stars show historic seismicity during the last 2,000 years according to Ambraseys (2002). (b) Repeater sequence centroids previously identified along the Western part of the MMF (Bohnhoff, Wollin, et al., 2017; Schmittbuhl et al., 2016; Uchida et al., 2019) indicated by blue triangles, green circles and red pentagrams, respectively. Depicted region is indicated by gray rectangle in subfigure (a). (c) Plate tectonic setting and GPS-derived velocities relative to stable Eurasia (Reilinger et al., 2006). Small gray rectangle indicates location of subfigure (a). (d) Map of the study region with events of the newly derived earthquake catalog (black dots), subregions for repeater identification (dashed rectangles) and centroids of repeater sequences reported here (red circles). Circle sizes scaled by the number of sequence members. White star identifies repeater sequence shown in Figure 2. Beachballs show fault plane solutions and corresponding epicenters of three events with $M_w \geq 5$ during the study period (Global CMT Catalog, Ekström et al., 2012; Dziewonski et al., 1981). Triangles and inverted triangles indicate stations from different seismic networks used in this study: GF, GONAF Network; PZ, PIRES Network; KO, Kandilli Observatory Network; TU, Turkish National Seismic Network; TB, MRC Earth and Marine Sciences Network; TL, Armutlu Local Seismic Network. Subregions for repeater identification: TeB, Tekirdağ Basin; WH, Western High; CB, Central Basin; KB, Kumburgaz Basin; IW, Istanbul West; IE, Istanbul East; CE, Cinarcik East; AP, Armutlu Peninsula; GG, Gulf of Gemlik.

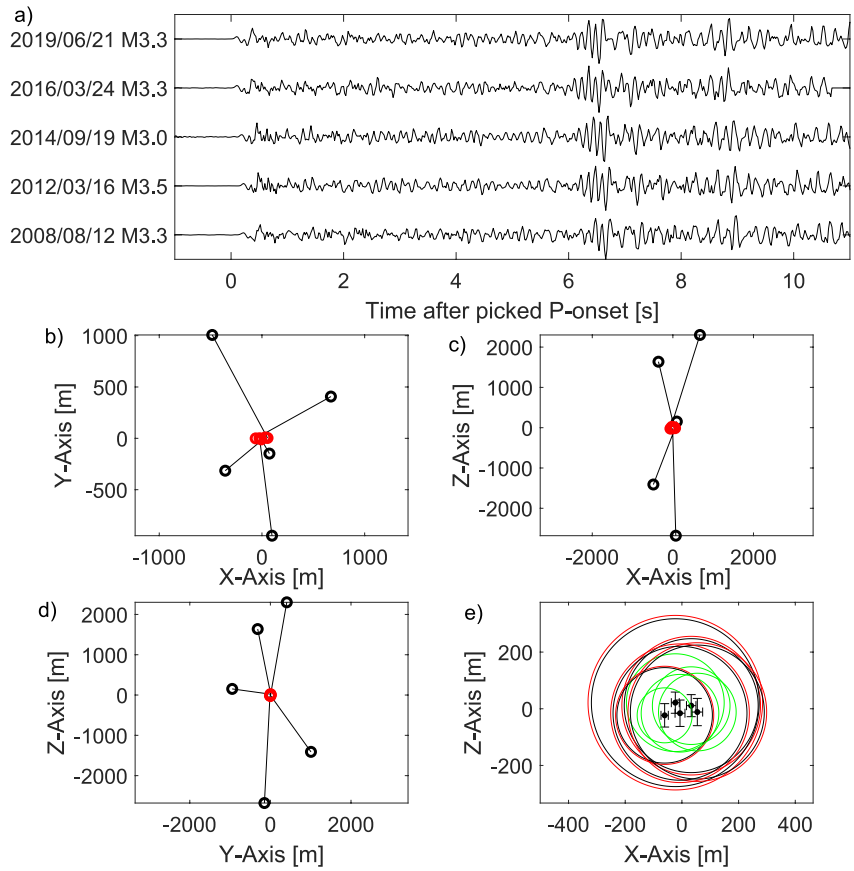

Figure 2. Example of a repeater sequence. (a) Vertical-component waveforms filtered between 2 and 20 Hz at station SLVT (see Figure 1d for station and repeater location). (b–d) Map view and x–z and y–z cross sections, respectively, of relative relocations (red circles) and single event locations (black circles). (e) Estimated rupture areas for an assumed rupture surface on a vertical E–W trending fault using a Brune source model (red), Madariaga model (green) and an empirical model for crustal earthquakes (black). Black error bars indicate formal errors from hypoDD.

3.3. Cumulative Seismic Slip

We estimate the cumulative seismic slip of a repeater sequence by summing up the contribution of each event, with magnitude M_i, in that sequence using an empirical slip-magnitude relation (Bohnhoff et al., 2010; their Table 1):

$$s_i = 10^{\log_{10}(4\cdot10^{-4})+0.5\cdot M_i}. \quad (1)$$

To obtain a seismic slip rate (SR), we apply two different estimations. In the first, we divide the cumulative slip of all sequence members by the complete observation interval (ΔT) of 15 years:

$$\mathrm{SR_a} = \frac{\sum_{i=1}^{N} s_i}{\Delta T}. \quad (2)$$

In the second, we divide the mean slip of the repeater events by the mean return period which is obtained by dividing the time interval of repeater activity ΔT_r by the number of inter-event times $N-1$ (see Equation 3 in Waldhauser & Schaff, 2021):

$$\mathrm{SR_b} = \frac{\sum_{i=1}^{N} s_i}{\Delta T_r\, N/(N-1)}. \quad (3)$$

See Text S3 in Supporting Information S1 for additional information. Finally, we divide this seismic SR by the long-term geodetic SR of the NAFZ in the region of the MMF of 15 mm/a (Hergert & Heidbach, 2011; Reilinger

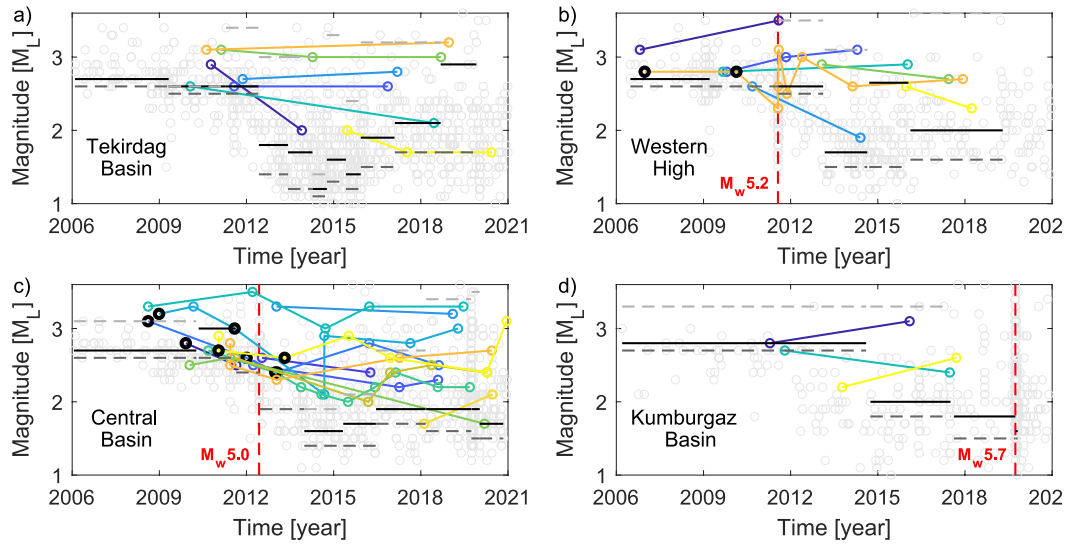

Figure 3. Magnitude-time distribution of repeater events along the Main Marmara Fault segments Tekirdağ Basin (a), Western High (b), Central Basin (c), and Kumburgaz Basin (d). Events belonging to the same sequence are plotted with the same color and connected by a line. Solid black and dashed dark and light gray lines indicate the maximum likelihood estimates of M_c for the investigated time periods and its 10th and 90th percentile, respectively, as obtained from a bootstrap Goodness-of-Fit approach (Wiemer & Wyss, 2000) for 80 consecutive events and 1,000 bootstrap runs. Light gray circles show local seismicity from our newly derived seismicity catalog, vertical red lines indicate the origin time of the 2011 M_w 5.2 event in WH (b), the 2012 M_w 5.0 event in CB (c) and the 2019 M_w 5.7 event in KB (d), respectively. Black filling of repeater events in (b) and (c) indicates repeater events also identified by Uchida et al. (2019).

et al., 2006) to obtain the fraction of creep, that is, the fraction of slip that is accommodated by creep in the area surrounding the respective repeater sequence. For the WH and CB sections, the maximum values of the fraction of creep reach nearly 50% when using Equation 3 (red circles in Figure 4a) and slightly less when using Equation 2 (black circles in Figure 4a). However, a considerable variability in the derived creep fraction is observed for repeater sequences in these regions. Laboratory (e.g., Summers & Byerlee, 1977) and modeling studies (e.g., Chen & Lapusta, 2009; Rubino et al., 2022) indicate that asperities can also show a creep-slip behavior with strain hardening alternating with seismic slip. In addition, it is also possible that creep and the corresponding repeater sequences take place on distinct subparallel strands as suggested for the San Andreas fault near Parkfield (Waldhauser et al., 2004). This might partly explain the scatter seen in Figure 4a for similar longitudinal positions. Another important parameter is the earthquake stress drop of the repeater events. Here, a constant stress drop of 3 MPa from ongoing studies in the region has been used. However, a variable stress drop would also alter our estimates of the seismic slip, with a doubling of the stress drop leading to a nearly 60% increase in slip, when other parameters are kept constant in a standard crack model (Uchida, 2019).

Toward the west (TeB) and east (KB) the derived fractions of creep are significantly smaller and do not exceed 25%. This observation is in good accordance with a previously reported locked status of the onshore Ganos fault immediately to the west of the MMF (Motagh et al., 2007).

The depth distribution of repeaters (and the overall seismicity) in the Tekirdağ Basin (Figure 4c) agrees with a locking depth of about 7–10 km. Comparable repeater depths are also found in the Kumburgaz Basin. This agrees with locking depths suggested by geodetic modeling for the Tekirdağ Basin and the MMF segment east of 28.5°E (Yılmaz et al., 2022). In the interval 27.7°E–28.1°E along the MMF our results suggest the absence of plate locking at shallow depths in agreement with offshore geodetic studies (Yamamoto et al., 2019).

3.4. Transient Acceleration of Repeater Sequence in Response to a Nearby M_w 5.2 Earthquake

In the WH region we observe a nine-member sequence close to the hypocenter of the 25 July 2011 M_w 5.2 event (Figures 1d and 3b). The recurrence period ($T_{ri} = t_{i+1} - t_i$) of two consecutive member events i and $i + 1$ is modified by the occurrence of the nearby M_w 5.2 event (Figures 3b and 4a). Plotting the inverse of

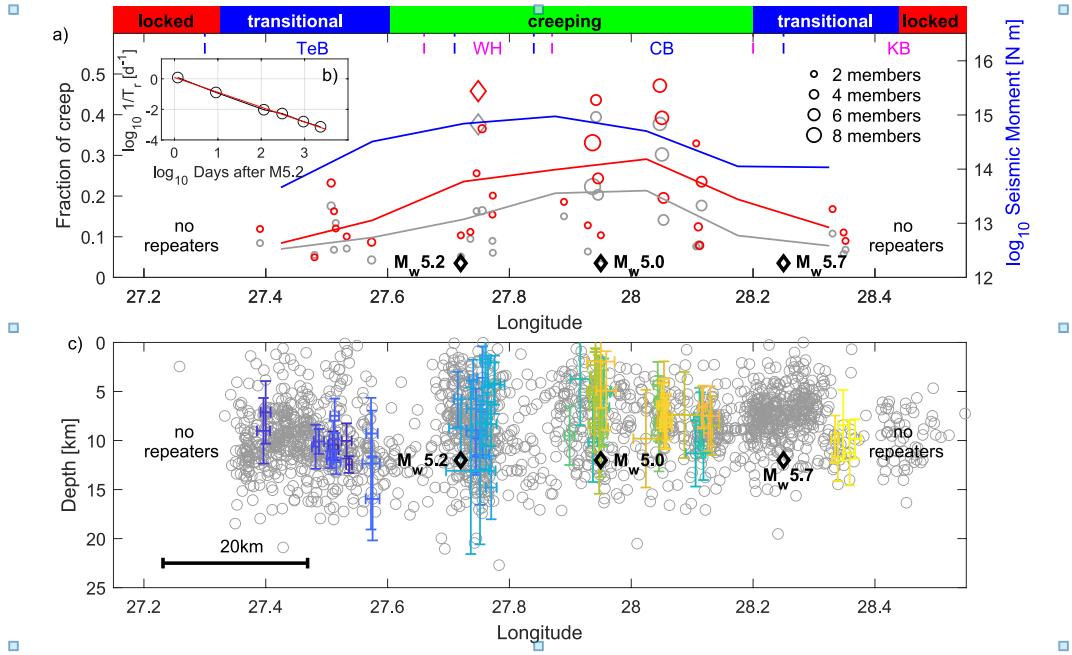

Figure 4. Longitudinal repeater variability along the Main Marmara Fault (MMF). (a) Along-fault (EW-trending) variation of the fraction of creep, with zero and one representing fully locked and creeping, respectively. Two estimates of the slip rate (SR) are shown: SR_a (gray) and SR_b (red) (see Equations 2 and 3). Longitude position of circles corresponds to the centroid of the repeater sequences and size scales with the number of sequence members. Red and gray diamonds indicate sequence responding to the nearby M_w 5.2 event. Black diamonds indicate locations of the M_w 5.2 event in 2011, the M_w 5.0 event in 2012, and the M_w 5.7 event in 2019. Red and gray lines indicate the mean fraction of creep along the MMF within 0.15° bins as estimated following Equations 2 and 3, respectively. Blue line indicates the cumulative seismic moment estimated from the magnitudes of all repeater events within the respective 0.15° bin. The spatial extent of investigated sections is indicated at the top. (b) Log-log representation of inverse recurrence interval as a function of time after M_w 5.2 event for the repeater sequence that responded to the mainshock occurrence. The linear regression line (red) indicates a power law time decay with $t^{-0.97}$. (c) Longitude-depth section of catalog events occurring in the repeater region. Gray circles indicate events with at least eight phase readings, rms ≤0.4s and major error-ellipsoid half axis ≤10 km from final NLLoc locations. Colored error bars indicate errors for repeater sequence members. Same color indicates same sequence. Black diamonds indicate positions of $M_w \geq 5$ events as given in the Global CMT catalog (Dziewonski et al., 1981; Ekström et al., 2012).

the recurrence period ($1/T_{ri}$) of sequence members after the main shock over time in a log-log plot (Figure 4b) reveals a power law behavior with $T_r \sim t^{-0.97}$ where t is time after the occurrence of the M_w 5.2 event. This behavior was for example, also observed for repeater sequences after the Loma Prieta earthquake (Schaff et al., 1998) and in several other repeater sequences in California (Waldhauser & Schaff, 2021) or Japan (Uchida & Matsuzawa, 2013).

This observation could either be explained by afterslip of the M_w 5.2 event or postseismic deformation under a power-law rheology (Schaff et al., 1998). The rupture radius of the M_w 5.2 event is a few km and the overlap with the asperity associated with the repeater sequence is in the order of the location and fault patch uncertainty. Thus, the repeater sequence could lie either on the same fault as the main shock but in a sufficient lateral offset to not have been ruptured by the same, or the asperity lies on a different fault. Interestingly, two other nearby repeater sequences did not respond similarly to the M_w 5.2 event (Figure 3b). This might either indicate a high spatial variability of postseismic slip close to the M_w 5.2 event or that these asperities ruptured during the main event and did not experience a comparable postseismic deformation. The M_w 5.7 event in KB segment and the M_w 5.0 event in the CB segment did not produce any immediate activity in the repeater sequences (Figures 3c and 3d). In the former case this might be due to the reverse-faulting mechanism of the event or the larger distance of the repeater sequences (Figure 1d). In the latter case, a southward dipping plane with normal faulting component as possible fault-plane (Figure 1d) might indicate an event on a subsidiary fault accommodating some of the extensional dynamics in the Marmara Sea. It is thus possible, that this event did not occur on the main branch of the MMF where the repeater sequences might be located.

4. Discussion and Conclusions

The presence of creeping sections at transform faults tapering off toward locked segments and leading to spatial variability in the accumulated slip deficit has been observed for example, in California (Scott et al., 2020; Toké & Arrowsmith, 2006) and Sumatra (Tong et al., 2018). The transitional segments are capable of hosting intermediate magnitude earthquakes like the Parkfield sequence in California and are actively accumulating slip deficits (Scott et al., 2020; Toké & Arrowsmith, 2006). Thus, a creeping section moving at velocities smaller than the long-term tectonic SR might still accumulate strain energy that can be released in a future earthquake (Tong et al., 2018). In this sense, the novel identification of repeaters in the western portion of the MMF suggests a gradual tapering-off of creep from the Western High and Central Basin regions toward the east and west. While a considerable amount of relative plate motion along the MMF in the Western High and Central Basin is accommodated by creep (Figure 4a) and thus partly releasing strain energy, the MMF sections toward the west and east are likely fully locked. A future large earthquake will likely nucleate either in a completely locked region or in the transition region from creeping to locked segments of the fault (e.g., Chaussard et al., 2015; Uchida & Bürgmann, 2019). Rupture initiation on the transitional creeping segments would affect more strongly the nearest locked fault patches. For instance, rupture at the Tekirdağ creeping transition would most likely proceed westwards to rupture the Ganos fault and thus away from Istanbul. Vice versa a rupture initiation at the Kumburgaz basin creep transition would cause the rupture to propagate eastwards toward Istanbul generating subsequently higher seismic risk. Rupture initiation is also likely on the locked fault segments, that is, the onshore Ganos fault and the offshore MMF east of longitude 28.4, including the Princes Island segment immediately south of Istanbul. Finally, it is also possible for a rupture to jump onto the creeping section in the Central Basin and Western High as a result of coseismic dynamic weakening (Noda & Lapusta, 2013) and release strain energy in the creeping section accumulated due to creep rates below the long-term tectonic SR. In that case, most of or even the entire current seismic gap would rupture in one single event reaching a magnitude of up to ~M_w 7.4.

Data Availability Statement

The newly compiled earthquake catalog of the Marmara region presented in this study is available under https://doi.org/10.5880/GFZ.4.2.2023.002. Waveform data used to create this catalog was acquired from the Turkish National Seismic Network (Disaster and Emergency Management Authority, 1990), Kandili Observatory Network (Kandilli Observatory and Earthquake Research Institute, Boğaziçi University, 1971), Princes Island Network (GFZ Potsdam, BU-Kandilli, 2006), MRC Earth and Marine Sciences Network (TÜBITAK Marmara Research Center, 2016) and GONAF borehole permanent network (Bohnhoff, Dresen, et al., 2017). Data processing, automatic phase picking and the creation of Figures 2–4 was done using Matlab (MATLAB, 2021). Single event earthquake localization was performed with version 7.0.0 of the NLLoc software available at http://alomax.free.fr/nlloc/. Relative earthquake relocalization was performed with hypoDD which is freely available at https://www.ldeo.columbia.edu/~felixw/hypoDD.html. Figure 1 was created using Generic Mapping Tools (GMT) version 6 (Wessel et al., 2019a, 2019b).

Acknowledgments
D.B. and P.M.G., acknowledge funding from the Helmholtz Association in the frame of the Young Investigators Group VH-NG-1232 (SAIDAN). Open Access funding enabled and organized by Projekt DEAL.

References

Ambraseys, N. (2002). The seismic activity of the Marmara sea region over the last 2000 years. *Bulletin of the Seismological Society of America*, *92*(1), 1–18. https://doi.org/10.1785/0120000843

Avouac, J.-P. (2015). From geodetic imaging of seismic and aseismic fault slip to dynamic modeling of the seismic cycle. *Annual Review of Earth and Planetary Sciences*, *43*(1), 233–271. https://doi.org/10.1146/annurev-earth-060614-105302

Barka, A., Akyuz, H. S., Altunel, E. R. H. A. N., Sunal, G., Cakir, Z., Dikbas, A., et al. (2002). The surface rupture and slip distribution of the 17 August 1999 Izmit earthquake (*M* 7.4), North Anatolian fault. *Bulletin of the Seismological Society of America*, *92*(1), 43–60. https://doi.org/10.1785/0120000841

Barka, A. A. (1992). The North Anatolian fault zone. Annales Tectonicae, VI supplement (pp. 164–195).

Becker, D., Martínez-Garzón, P., Wollin, C., Kılıç, T., & Bohnhoff, M. (2023). Homogenized regional seismicity catalogue for the Marmara region, northwestern Turkey, for the time interval 2006-2020. V. 1.0 [Dataset]. GFZ Data Services. http://doi.org/10.5880/GFZ.4.2.2023.002

Bohnhoff, M., Bulut, F., Dresen, G., Malin, P. E., Eken, T., & Aktar, M. (2013). An earthquake gap south of Istanbul. *Nature Communications*, *4*(1), 1999. https://doi.org/10.1038/ncomms2999

Bohnhoff, M., Dresen, G., Ceken, U., Kadirioglu, F. T., Kartal, R. F., Kilic, T., et al. (2017). GONAF—The borehole geophysical observatory at the North Anatolian fault in the eastern Sea of Marmara. *Scientific Drilling*, *22*, 19–28. https://doi.org/10.5194/sd-22-19-2017

Bohnhoff, M., Dresen, G., Ellsworth, W. L., & Ito, H. (2010). Passive seismic monitoring of natural and induced earthquakes: Case studies, future directions and socio-economic relevance. In S. Cloetingh & J. Negendank (Eds.), *New frontiers in integrated solid earth science, integrated year planet earth*. Springer. https://doi.org/10.1007/978-90-481-2737-5

Bohnhoff, M., Harjes, H.-P., & Meier, T. (2005). Deformation and stress regimes in the Hellenic subduction zone from focal Mechanisms. *Journal of Seismology*, *9*(3), 341–366. https://doi.org/10.1007/s10950-005-8720-5

Bohnhoff, M., Martinez-Garzon, P., Bulut, F., & Ben-Zion, Y. (2016). Maximum earthquake magnitudes along different sections of the North Anatolian fault zone. *Tectonophysics*, *674*, 147–165. https://doi.org/10.1016/j.tecto.2016.02.028

Bohnhoff, M., Wollin, C., Domigall, D., Küperkoch, L., Martínez-Garzón, P., Kwiatek, G., et al. (2017). Repeating Marmara Sea earthquakes: Indication for fault creep. *Geophysical Journal International*, *210*(1), 332–339. https://doi.org/10.1093/gji/ggx169

Brune, J. N. (1970). Tectonic stress and seismic shear waves from earthquakes. *Journal of Geophysical Research*, *75*(26), 4997–5009. https://doi.org/10.1029/jb075i026p04997

Bulut, F., Bohnhoff, M., Eken, T., Janssen, C., Kilic, T., & Dresen, G. (2012). The East Anatolian Fault Zone: Seismotectonic setting and spatio-temporal characteristics of seismicity based on precise earthquake locations. *Journal of Geophysical Research*, *117*(B7), B07304. https://doi.org/10.1029/2011JB008966

Chaussard, E., Bürgmann, R., Fattahi, H., Johnson, C. W., Nadeau, R., Taira, T., & Johanson, I. (2015). Interseismic coupling and refined earthquake potential on the Hayward-Calaveras fault zone. *Journal of Geophysical Research: Solid Earth*, *120*(12), 8570–8590. https://doi.org/10.1002/2015jb012230

Chen, T., & Lapusta, N. (2009). Scaling of small repeating earthquakes explained by interaction of seismic and aseismic slip in a rate and state fault model. *Journal of Geophysical Research*, *114*(B1), B01311. https://doi.org/10.1029/2008jb005749

Di Giacomo, D., Engdahl, E. R., & Storchak, D. A. (2018). The ISC-GEM earthquake catalogue (1904–2014): Status after the extension project. *Earth System Science Data*, *10*(4), 1877–1899. https://doi.org/10.5194/essd-10-1877-2018

Disaster and Emergency Management Presidency. (1990). Turkish National seismic network [Dataset]. Department of Earthquake, Disaster and Emergency Management Presidency. http://doi.org/10.7914/SN/TU

Dziewonski, A. M., Chou, T.-A., & Woodhouse, J. H. (1981). Determination of earthquake source parameters from waveform data for studies of global and regional seismicity. *Journal of Geophysical Research*, *86*(B4), 2825–2852. https://doi.org/10.1029/JB086iB04p02825

Ekström, G., Nettles, M., & Dziewonski, A. M. (2012). The global CMT project 2004-2010: Centroid-moment tensors for 13,017 earthquakes. *Physics of the Earth and Planetary Interiors*, *200–201*, 1–9. https://doi.org/10.1016/j.pepi.2012.04.002

Ellsworth, W. L. (1995). Characteristic earthquakes and long-term earthquake forecasts: Implications of Central California Seismicity. In *Urban disaster mitigation: The role of engineering and technology* (pp. 1–14). https://doi.org/10.1016/B978-008041920-6/50007-5

Ergintav, S., Reilinger, R. E., Çakmak, R., Floyd, M., Cakir, Z., Doğan, U., et al. (2014). Istanbul's earthquake hot spots: Geodetic constraints on strain accumulation along faults in the Marmara seismic gap. *Geophysical Research Letters*, *41*(16), 5783–5788. https://doi.org/10.1002/2014gl060985

Flerit, F., Armijo, R., King, G., & Meyer, B. (2004). The mechanical interaction between the propagating North Anatolian Fault and the back-arc extension in the Aegean. *Earth and Planetary Science Letters*, *224*(3–4), 347–362. https://doi.org/10.1016/j.epsl.2004.05.028

Gao, D., Kao, H., & Wang, B. (2021). Misconception of waveform similarity in the identification of repeating earthquakes. *Geophysical Research Letters*, *48*(13), GL092815. https://doi.org/10.1029/2021GL092815

GFZ Potsdam, BU-Kandilli. (2006). Prince Islands Real-time earthquake monitoring system [Dataset]. International Federation of Digital Seismograph Networks. http://doi.org/10.7914/SN/PZ

Gholamrezaie, E., Scheck-Wenderoth, M., Cacace, M., Bott, J., Heidbach, O., Bohnhoff, M., & Strecker, M. R. (2021). Lithospheric strength variations and seismotectonic segmentation below the Sea of Marmara. *Tectonophysics*, *815*, 228999. https://doi.org/10.1016/j.tecto.2021.228999

Harris, R. A. (2017). Large earthquakes and creeping faults. *Reviews of Geophysics*, *55*(1), 169–198. https://doi.org/10.1002/2016RG000539

Hergert, T., & Heidbach, O. (2011). Slip-rate variability and distributed deformation in the Marmara Sea fault system. *Nature Geoscience*, *3*(2), 132–135. https://doi.org/10.1038/ngeo739

International Seismological Centre. (2022). ISC-GEM earthquake catalogue [Dataset]. NASA/ADS. http://doi.org/10.31905/d808b825

Kaduri, M., Gratier, J.-P., Renard, F., Çakir, Z., & Lasserre, C. (2016). The implications of fault zone transformation on aseismic creep: Example of the North Anatolian Fault, Turkey. *Journal of Geophysical Research: Solid Earth*, *122*(6), 4208–4236. https://doi.org/10.1002/2016JB013803

Kandilli Observatory and Earthquake Research Institute. (2022). Boğaziçi University Kandilli observatory and Earthquake Research Institute—Regional earthquake-Tsunami monitoring center [Dataset]. RETMC. Retrieved from http://www.koeri.boun.edu.tr/sismo/2/earthquake-catalog/

Kandilli Observatory and Earthquake Research Institute, Boğaziçi University. (1971). Kandilli observatory and Earthquake Research Institute (KOERI) [Dataset]. International Federation of Digital Seismograph Networks. http://doi.org/10.7914/SN/KO

Lange, D., Kopp, H., Royer, J., Henry, P., Çakir, Z., Petersen, F., et al. (2019). Interseismic strain build-up on the submarine North Anatolian fault offshore Istanbul. *Nature Communications*, *10*(1), 3006. https://doi.org/10.1038/s41467-019-11016-z

Le Pichon, X., Şengör, A. M. C., Kende, J., İmren, C., Henry, P., Grall, C., & Karabulut, H. (2016). Propagation of a strike-slip plate boundary within an extensional environment: The westward propagation of the North Anatolian fault. *Canadian Journal of Earth Sciences*, *53*(11), 1416–1439. https://doi.org/10.1139/cjes-2015-0129

Liu, Y.-K., Ross, Z. E., Cochran, E. S., & Lapusta, N. (2022). A unified perspective of seismicity and fault coupling along the San Andreas Fault. *Science Advances*, *8*(8), eabk1167. https://doi.org/10.1126/sciadv.abk1167

Lomax, A., Michelini, A., & Curtis, A. (2009). Earthquake location, direct, global-search methods, in complexity. In *Encyclopedia of complexity and system science, part 5* (pp. 2449–2473). Springer. https://doi.org/10.1007/978-0-387-30440-3

Lomax, A., Virieux, J., Volant, P., & Berge, C. (2000). Probabilistic earthquake location in 3D and layered models: Introduction of a Metropolis-Gibbs method and comparison with linear locations. In C. H. Thurber & N. Rabinowitz (Eds.), *Advances in seismic event location* (pp. 101–134). Kluwer.

Madariaga, R. (1976). Dynamics of an expanding circular fault. *Bulletin of the Seismological Society of America*, *66*(3), 639–666. https://doi.org/10.1785/bssa0660030639

MATLAB. (2021). *Version 9.10.0 (R2021a)*. The MathWorks Inc.

Moore, D. E., & Lockner, D. A. (2013). Chemical controls on fault behavior: Weakening of serpentinite sheared against quart-bearing rocks and its significance for fault creep in the San Andreas system. *Journal of Geophysical Research: Solid Earth*, *118*(5), 1–13. https://doi.org/10.1002/jgrb.50140

Motagh, M., Hoffmann, J., Kampes, B., Baes, M., & Zschau, J. (2007). Strain accumulation across the Gazikoy–Saros segment of the North Anatolian Fault inferred from Persistent Scatterer Interferometry and GPS measurements. *Earth and Planetary Science Letters*, *255*(3–4), 432–444. https://doi.org/10.1016/j.epsl.2007.01.003

Murru, M., Akinci, A., Falcone, G., Pucci, S., Console, R., & Parsons, T. (2016). $M \geq 7$ earthquake rupture forecast and time dependent probability for the Sea of Marmara region, Turkey. *Journal of Geophysical Research: Solid Earth*, *121*(4), 2679–2707. https://doi.org/10.1002/2015JB012595

Noda, H., & Lapusta, N. (2013). Stable creeping fault segments can become destructive as a result of dynamic weakening. *Nature*, *493*(7433), 518–521. https://doi.org/10.1038/nature11703

Parsons, T. (2004). Recalculated probability of $M \geq 7$ earthquakes beneath the Sea of Marmara, Turkey. *Journal of Geophysical Research*, *109*(B5), B05304. https://doi.org/10.1029/2003JB002667

Poupinet, G., Ellsworth, W. L., & Frechet, J. (1984). Monitoring velocity variations in the crust using earthquake doublets: An application to the Calaveras Fault, California. *Journal of Geophysical Research*, *89*(B7), 5719–5731. https://doi.org/10.1029/JB089iB07p05719

Reilinger, R., McClusky, S., Vernant, P., Lawrence, S., Ergintav, S., Cakmak, R., et al. (2006). GPS constraints on continental deformation in the Africa-Arabia-Eurasia continental collision zone and implications for the dynamics of plate interactions. *Journal of Geophysical Research*, *111*(B5), 2156–2202. https://doi.org/10.1029/2005JB004051

Reilinger, R. E., Ergintav, S., Burgmann, R., McClusky, S., Lenk, O., Barka, A., et al. (2000). Coseismic and postseismic fault slip for the 17 August 1999, $M = 7.5$, Izmit, Turkey earthquake. *Science*, *289*(5484), 1519–1524. https://doi.org/10.1126/science.289.5484.1519

Rubino, V., Lapusta, N., & Rosakis, A. J. (2022). Intermittent lab earthquakes in dynamically weakening fault gouge. *Nature*, *606*(7916), 1–8. https://doi.org/10.1038/s41586-022-04749-3

Schaff, D. P., Beroza, G. C., & Shaw, B. E. (1998). Postseismic response of repeating aftershocks. *Geophysical Research Letters*, *25*(24), 4549–4552. https://doi.org/10.1029/1998GL900192

Schmittbuhl, J., Karabulut, H., Lengliné, O., & Bouchon, M. (2016). Long-lasting seismic repeaters in the central basin of the main Marmara fault. *Geophysical Research Letters*, *43*(18), 9527–9534. https://doi.org/10.1002/2016GL070505

Scott, C. P., DeLong, S. B., & Arrowsmith, J. R. (2020). Distribution of aseismic deformation along the Central San Andreas and Calaveras faults from differencing repeat airborne lidar. *Geophysical Research Letters*, *47*(22), e2020GL090628. https://doi.org/10.1029/2020GL090628

Sengör, A. M. C., Tuysuz, O., Imren, C., Sakinc, M., Eyidogan, H., Gorur, G., et al. (2005). The North Anatolian Fault: A new look. *Annual Review of Earth and Planetary Sciences*, *33*(1), 37–112. https://doi.org/10.1146/annurev.earth.32.101802.120415

Stein, R. S., Barka, A. A., & Dieterich, J. H. (1997). Progressive failure on the North Anatolian fault since 1939 by earthquake stress triggering. *Geophysical Journal International*, *128*(3), 594–604. https://doi.org/10.1111/j.1365-246X.1997.tb05321.x

Storchak, D. A., Di Giacomo, D., Bondár, I., Engdahl, E. R., Harris, J., Lee, W. H. K., et al. (2013). Public release of the ISC-GEM global instrumental earthquake catalogue (1900–2009). *Seismological Research Letters*, *84*(5), 810–815. https://doi.org/10.1785/0220130034

Storchak, D. A., Di Giacomo, D., Engdahl, E. R., Harris, J., Bondár, I., Lee, W. H. K., et al. (2015). The ISC-GEM global instrumental earthquake catalogue (1900–2009): Introduction. *Physics of the Earth and Planetary Interiors*, *239*, 48–63. https://doi.org/10.1016/j.pepi.2014.06.009

Summers, R., & Byerlee, J. (1977). Summary of results of frictional sliding studies, at confining pressures up to 6.98 kb, in select rock materials. *U.S. Geological Survey Open-File Report*, *77–142*, 129.

Toké, N. A., & Arrowsmith, J. R. (2006). Reassessment of a slip budget along the Parkfield segment of the San Andreas fault. *Bulletin of the Seismological Society of America*, *96*(4B), 339–348. https://doi.org/10.1785/0120050829

Tong, X., Sandwell, D. T., & Schmidt, D. A. (2018). Surface creep rate and moment accumulation rate along the Aceh segment of the Sumatran fault from L-band ALOS-1/PALSAR-1 observations. *Geophysical Research Letters*, *45*(8), 3404–3412. https://doi.org/10.1002/2017GL076723

TÜBITAK Marmara Research Center. (2016). MRC Earth and marine Sciences network [Dataset]. International Federation of Digital Seismograph Networks. http://doi.org/10.7914/SN/TB

Uchida, N. (2019). Detection of repeating earthquakes and their application in characterizing slow fault slip. *Progress in Earth and Planetary Science*, *6*(1), 40. https://doi.org/10.1186/s40645-019-0284-z

Uchida, N., & Bürgmann, R. (2019). Repeating earthquakes. *Annual Review of Earth and Planetary Sciences*, *47*(1), 305–332. https://doi.org/10.1146/annurev-earth-053018-060119

Uchida, N., Kalafat, D., Pinar, A., & Yamamoto, Y. (2019). Repeating earthquakes and interplate coupling along the western part of the North Anatolian Fault. *Tectonophysics*, *769*, 228185. https://doi.org/10.1016/j.tecto.2019.228185

Uchida, N., & Matsuzawa, T. (2013). Pre- and postseismic slow slip surrounding the 2011 Tohoku-oki earthquake rupture. *Earth and Planetary Science Letters*, *374*, 81–91. https://doi.org/10.1016/j.epsl.2013.05.021

Waldhauser, F., & Ellsworth, W. L. (2000). A double-difference earthquake location algorithm: Method and application to the northern Hayward fault. *Bulletin of the Seismological Society of America*, *90*(6), 1353–1368. https://doi.org/10.1785/0120000006

Waldhauser, F., Ellsworth, W. L., Schaff, D. P., & Cole, A. (2004). Streaks, multiplets, and holes: High-resolution spatiotemporal behavior of Parkfield seismicity. *Geophysical Research Letters*, *31*, 18. https://doi.org/10.1029/2004GL020649

Waldhauser, F., & Schaff, D. P. (2021). A comprehensive search for repeating earthquakes in northern California: Implications for fault creep, slip rates, slip partitioning, and transient stress. *Journal of Geophysical Research: Solid Earth*, *126*(11), e2021JB022495. https://doi.org/10.1029/2021JB022495

Wessel, P., Luis, J. F., Uieda, L., Scharroo, R., Wobbe, F., Smith, W. H. F., & Tian, D. (2019a). The generic mapping tools version 6 [Software]. Zenodo (Funded by US National Science Foundation grants OCE-1558403 and EAR-1829371). http://doi.org/10.5281/zenodo.3407866

Wessel, P., Luis, J. F., Uieda, L., Scharroo, R., Wobbe, F., Smith, W. H. F., & Tian, D. (2019b). The generic mapping tools version 6. *Geochemistry, Geophysics, Geosystems*, *20*(11), 5556–5564. https://doi.org/10.1029/2019gc008515

Wiemer, S., & Wyss, M. (2000). Minimum magnitude of complete reporting in earthquake catalogs: Examples from Alaska, the Western United States, and Japan. *Bulletin of the Seismological Society of America*, *90*(4), 859–869. https://doi.org/10.1785/0119990114

Wollin, C., Bohnhoff, M., Martinez Garzon, P., Küperkoch, L., & Raub, C. (2018). A unified earthquake catalogue for the Sea of Marmara region, Turkey, based on automatized phase picking and traveltime inversion: Seismotectonic implications. *Tectonophysics*, *747–748*, 416–444. https://doi.org/10.1016/j.tecto.2018.05.020

Yamamoto, R., Kido, M., Ohta, Y., Takahashi, N., Yamamoto, Y., Pinar, A., et al. (2019). Seafloor geodesy revealed partial creep of the North Anatolian Fault submerged in the Sea of Marmara. *Geophysical Research Letters*, *46*(3), 1268–1275. https://doi.org/10.1029/2018GL080984

Yılmaz, Z., Konca, A. O., & Ergintav, S. (2022). The effect of the 3-D structure on strain accumulation and the interseismic behavior along the North Anatolian Fault in the sea of Marmara. *Journal of Geophysical Research: Solid Earth*, *127*(3), e2021JB022838. https://doi.org/10.1029/2021JB022838

References From the Supporting Information

Beyreuther, M., Barsch, R., Krischer, L., Megies, T., Behr, Y., & Wassermann, J. (2010). ObsPy: A Python toolbox for seismology. *Seismological Research Letters*, *81*(3), 530–533. https://doi.org/10.1785/gssrl.81.3.530

Karabulut, H., Schmittbuhl, J., Ozalaybey, S., Lengliné, O., Kömeç-Mutlu, A., Durand, V., et al. (2011). Evolution of the seismicity in the eastern Marmara Sea a decade before and after the 17 August 1999 Izmit earthquake. *Tectonophysics*, *510*(1–2), 17–27. https://doi.org/10.1016/j.tecto.2011.07.009